Perturbation and asymptotic solutions of energy localization of impurity modes in a one-dimensional anharmonic chain

Xuan-Lin Chen,[1] Gang-Bei Zhu,[2] Ze-Hui Jiang,[1] and Yan-Qiang Yang[1,2,*]

[1]*Department of Physics, Harbin Institute of Technology, Harbin 150001, Heilongjiang Province, China*

[2]*National Key Laboratory of Shock Wave and Detonation Physics, Institute of Fluid Physics, China Academy of Engineering Physics, Mianyang 621900, Sichuan Province, China*

(Received 10 June 2017; revised manuscript received 27 August 2017; published 13 October 2017)

A 1D anharmonic chain with a single impurity particle is used to study the vibrational energy localization. Numerical and asymptotic solutions for the symmetric anharmonic localized mode are both presented. The numerical results reveal that the energy localization strengthens with decreasing impurity mass or with increasing anharmonicity. In the weak-anharmonicity limit, the energy localization is close to the harmonic results and varies linearly with respect to the anharmonicity parameter. In the strong-anharmonicity limit, the localized structure tends towards a constant value that is independent of anharmonicity, but as a function of impurity mass. We finally analyze the stability of this symmetric impurity mode, and evidence a stable asymmetric mode as the result of a bifurcation from the symmetric mode for the case of the large impurity mass.

DOI: 10.1103/PhysRevB.96.144107

I. INTRODUCTION

The study of energy localization of impurity modes in a harmonic lattice is well known [1]. Depending on the mass of the impurity and bonding to the host neighbors, the frequency of impurity modes always lies outside the phonon spectrum. Spatially localized modes may also exist in perfect anharmonic lattices. Such modes in chains were first observed by A. M. Kosevich and A. S. Kovalev [2]. The asymptotic solution of a solitonlike mode was obtained, restricted to the small-amplitude vibrations and the frequency was close to the top of the phonon spectrum [2]. By contrast, the study of the large-amplitude vibrations by Sievers and Takeno described a symmetric small-size localized mode (the ST mode) [3] with an oscillation center located at a particle site, while Page found another mode (the Page mode) with an oscillation center located midway between two neighboring particle sites [4]. These latter two distinct types of localized modes are called intrinsic localized modes (ILMs) or discrete breathers (DBs), and are considered to relate to the effective periodic Peierls-Nabarro (PN) potential [5]. The ST mode's center is located at the top of the PN potential, while that of the Page mode is at the bottom of the PN potential.

The combination of the ILM and the impurity mode is called anharmonic impurity mode. As defects seem ubiquitous in a real lattice system, the investigation of anharmonic impurity modes in the nonlinear system becomes essential. The presence of impurities can drastically change the properties of localized modes. An ILM may be affected by impurities because it is a characteristically "discrete" phenomenon that is caused by the discreteness of lattices with adjacent particles vibrating in opposite directions over time. Some applications have even extended into biology: the anharmonic impurity mode has been postulated to act as a precursor of a reaction, e.g., DNA denaturation [6]. Moreover, it provides a kind of hot spot that is similar to the nonimpurity breather hot spot [7,8].

Kivshar *et al.* investigated the patterns of anharmonic impurity modes 20 years ago and found strongly localized impurity modes localized on three or four particles in the large-amplitude limit [9]. Later, they found a solution for the localized mode with a heavy impurity [5]. Sarkar examined that a light-mass impurity mode fulfills nonresonance with the linear (or phonon) spectrum because its frequency is located above the phonon band whereas the frequency of a heavy-mass impurity mode drops into the phonon band [10].

The present paper will explore in detail the quantitative dependence of the vibrational energy localization of the localized mode on the impurity mass and the anharmonic vibrational parameter—a connection that has not been fully investigated. Specifically, this paper presents numerical and asymptotic solutions for the energy localization and the frequency of the symmetric anharmonic impurity mode in a 1D anharmonic chain, in both the weak-anharmonicity limit and strong-anharmonicity limit. These solutions show that the energy localization strengthens with decreasing impurity mass or with increasing anharmonicity. We also discuss stabilities of both asymmetric and symmetric modes based on the results of numerical solutions and present the relationship between a critical value of the impurity mass and the frequency of the impurity mode. This critical value will be described in Sec. III C in detail.

II. THEORY MODEL

We consider a simple but rather fundamental chain, the Fermi-Pasta-Ulam (FPU) chain [11], in which any particle only interacts with its nearest-neighbor particles. This 1D anharmonic chain has a harmonic component and a quartic anharmonic component, and the equation of motion of the chain is expressed as

$$m_n\ddot{u}_n = -k_2(2u_n - u_{n+1} - u_{n-1}) - k_4[(u_n - u_{n+1})^3 + (u_n - u_{n-1})^3], \quad (1)$$

where k_2 and k_4 are the harmonic and quartic force constants, respectively, u_n is the displacement of the nth particle, and

*Corresponding author: yqyang@hit.edu.cn

m_n is the mass of the nth particle. The cubic anharmonic term $k_3[(u_n - u_{n+1})^2 + (u_n - u_{n-1})^2]$, which is mainly related to thermal expansion, plays a negligible role in the localization process [12]. The main contribution of the cubic anharmonicity is the compression and rarefaction of the 1D anharmonic chain. We seek a stationary solution to Eq. (1) by setting

$$u_n = \varphi_n \cos(\omega t), \tag{2}$$

where φ_n is the vibrational amplitude of the nth particle. When we substitute Eq. (2) into Eq. (1) and use the rotating wave approximation [13], in which we have $\cos^3(\omega t) \approx \frac{3}{4}\cos(\omega t)$ and $\cos^2(\omega t) \approx 1/2$, Eq. (1) then becomes

$$m_n\omega^2\varphi_n = k_2(2\varphi_n - \varphi_{n+1} - \varphi_{n-1}) + \frac{3k_4}{4}[(\varphi_n - \varphi_{n+1})^3 + (\varphi_n - \varphi_{n-1})^3]. \tag{3}$$

Because adjacent particles vibrate in opposite directions in the impurity mode [14], we introduce the slowly varying oscillation envelope v_n as shown in Eq. (4),

$$\varphi_n = \varphi_0(-1)^n v_n, \tag{4}$$

where φ_0 is the vibrational amplitude of the impurity. Eq. (3) then becomes

$$\frac{m_n}{m}\varpi^2 v_n = (2v_n + v_{n+1} + v_{n-1}) + f[(v_n + v_{n+1})^3 + (v_n + v_{n-1})^3], \tag{5}$$

where $m_n = m(n \neq 0)$ is the mass of the host particle, $m_0 = M$ is the mass of the impurity, $\varpi = \sqrt{\frac{m}{k_2}}\omega$ is an effective frequency parameter, and $f = \frac{3k_4}{4k_2}\varphi_0{}^2$ is the anharmonicity parameter.

III. ANHARMONIC IMPURITY MODES

The harmonic impurity mode can be analytically determined. For a light-mass impurity, such mode has a frequency above the upper cutoff $\varpi_m = 2$ of the linear spectrum, whereas for a heavy-mass impurity, the mode has frequency lying below the cutoff [1]. The solution of the harmonic light-mass impurity is

$$v_n = \left(\frac{\lambda}{2-\lambda}\right)^{|n|}, \tag{6}$$

$$\varpi^2 = \frac{4}{(2-\lambda)\lambda}, \tag{7}$$

where $\lambda = M/m$ is the mass ratio parameter.

A. Weak-anharmonicity limit

In the limit where $f \to 0$, the perturbation method is used. We set the perturbation solution to be

$$v_0 = 1, \tag{8}$$

$$v_n = \left[\frac{\lambda}{2-\lambda} + O_n(f)\right]v_{n-1} \text{ for } n > 0, \tag{9}$$

$$\varpi^2 = \frac{4}{(2-\lambda)\lambda} + \Omega(f), \tag{10}$$

where $O_n(f)$ and $\Omega(f)$ are the first-order perturbation term of v_n and ϖ^2, respectively. Equation (5) then becomes a set of linear equations. For $n = 0$,

$$\frac{\lambda}{2}\Omega(f) - O_1(f) = f\left(1 + \frac{\lambda}{2-\lambda}\right)^3, \tag{11}$$

for $n \neq 0$,

$$\left(\frac{2-\lambda}{\lambda}\right)^2 O_n(f) - O_{n+1}(f) + \Omega(f) = f\left(\frac{\lambda}{2-\lambda}\right)^{2n-3}\left(\frac{\lambda}{2-\lambda} + 1\right)^3\left[1 + \left(\frac{\lambda}{2-\lambda}\right)^3\right], \tag{12}$$

The fact that this set of equations is linear means that $O_n(f)$ and $\Omega(f)$ are both proportional to f. As a special case, we set $(\frac{\lambda}{2-\lambda})^{2n-3} \to 0$ for $n > 2$ [e.g., $\lambda < 0.4$, and $(\frac{\lambda}{2-\lambda})^3 < 0.016$], and we obtain

$$O_{n+1}(f) = \left(\frac{2-\lambda}{\lambda}\right)^2 O_n(f) + \Omega(f) \quad \text{for } n > 2, \tag{13}$$

which means that $O_{n+1}(f) \geqslant O_n(f)$. If $O_{n+1}(f) > O_n(f)$, then $O_{n+1}(f)$ will not be convergent for $(\frac{2-\lambda}{\lambda})^{2n} \to \infty$; therefore the convergent condition is $O_{n+1}(f) = O_n(f)$ and we obtain

$$O_n(f) = \frac{\lambda^2}{4(\lambda-1)}\Omega(f). \tag{14}$$

We then solve the linear equation and drop the higher-order terms ($n > 2$) of the Taylor expansion to give

$$\Omega(f) \cong \frac{f}{4\lambda}(8 + 12\lambda + 10\lambda^2 + 5\lambda^3), \tag{15}$$

$$O_1(f) \cong -\frac{f\lambda^2}{4}, \tag{16}$$

$$O_2(f) \cong -\frac{f\lambda}{4}(2 + 5\lambda), \tag{17}$$

$$O_n(f) = O_3(f) \cong -\frac{f\lambda}{4}(2 + 5\lambda) \cong O_2(f). \tag{18}$$

The perturbation solutions are as follows:

$$v_0 = 1, \tag{19}$$

$$v_n \cong \left(\frac{\lambda}{2-\lambda} - \frac{f\lambda^2}{4}\right)\left[\frac{\lambda}{2-\lambda} - \frac{f\lambda}{4}(2 + 5\lambda)\right]^{|n|-1}, \tag{20}$$

$$\varpi^2 \cong \frac{4}{(2-\lambda)\lambda} + \frac{f}{4\lambda}(8 + 12\lambda + 10\lambda^2 + 5\lambda^3). \tag{21}$$

The total energy is given by Eq. (22) [15],

$$E_t = \frac{1}{2}\omega^2\varphi_0^2\sum_n v_n^2 m_n = \frac{2\,k_2^2}{3\,k_4}\varpi^2 f\sum_n v_n^2 m_n. \tag{22}$$

We consider the rate of energy localization as a ratio E_i/E_t which is expressed approximately as Eq. (23) according to the perturbation solution Eq. (20):

$$\frac{E_i}{E_t} = \frac{v_0^2 m_0}{\sum_n v_n^2 m_n} \cong \frac{2(1-\lambda)}{2-\lambda} + \frac{(4 - 2\lambda + 5\lambda^2)\lambda^2 f}{4(2-\lambda)}. \tag{23}$$

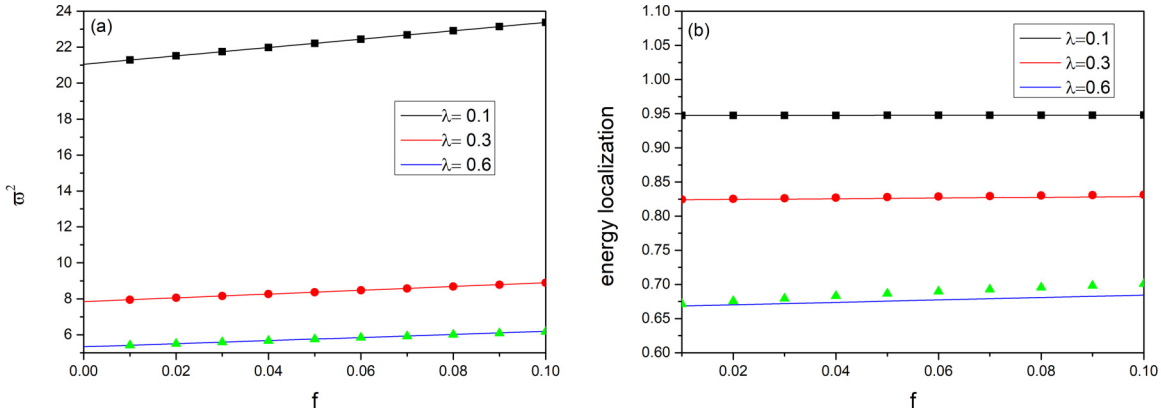

FIG. 1. Numerical solutions (points) and perturbation solutions (lines) for (a) ϖ^2 and (b) E_i/E_t at $\lambda = 0.1, 0.3$, and 0.6.

These perturbation solutions show that both ϖ^2 and E_i/E_t are linearly dependent on f. The harmonic results are obtained when $f = 0$. These perturbation solutions are then compared with the numerical results, as shown in Figs. 1 and 2. Figure 2 shows that the requirements on λ for the perturbation solution are stricter for E_i/E_t than for ϖ^2.

B. Strong-anharmonicity limit: strongly localized modes

In contrast to the weak-anharmonicity limit, impurity modes are localized to only a few particles when f is very large. Kivshar *et al.* reduced Eq. (5) to a few coupled equations to look for the solutions [5,9]. The authors found the stable asymmetric and symmetric patterns with only three or four particles for varying λ [5,9]. We will now use the asymptotic approach to extend the pattern to the whole chain.

Only the symmetric-type mode is considered here, and its equations are expressed as follows. For $n = 0$,

$$\lambda/2\ \varpi^2 = (1 + v_1) + f[(1 + v_1)^3], \tag{24}$$

and $n \neq 0$,

$$\varpi^2 v_n = (2v_n + v_{n+1} + v_{n-1}) + f[(v_n + v_{n+1})^3 + (v_n + v_{n-1})^3], \tag{25}$$

where $v_0 = 1$ because of its definition in Eq. (4).

When $f \to \infty$, the equations of motion given in Eqs. (24) and (25) take on the following simpler forms:

$n = 0$,

$$\frac{\varpi^2}{f} = \frac{(1 + v_1)^3}{\lambda/2}, \tag{26}$$

and $n \neq 0$,

$$\frac{\varpi^2 v_n}{f} = \frac{(1 + v_1)^3}{\lambda/2} v_n = (v_n + v_{n+1})^3 + (v_n + v_{n-1})^3. \tag{27}$$

Equation (26) gives the proportional relation between ϖ^2 and f.

The localization demands that $v_n < 1$ and $v_n > v_{n+1}$, and Eq. (27) must therefore satisfy its convergence conditions of $v_n \gg v_{n+1}$ for $n > 0$, and then takes the approximate form

$$\begin{aligned} &\frac{(1 + v_1)^3}{\lambda/2} v_1 \cong {v_1}^3 + (v_1 + 1)^3, \\ &\frac{(1 + v_1)^3}{\lambda/2} v_2 \cong {v_1}^3, \\ &\cdots\cdots\cdots\cdots\cdots\cdots \\ &\frac{(1 + v_1)^3}{\lambda/2} v_n \cong {v_{n-1}}^3. \\ &\cdots\cdots\cdots\cdots\cdots\cdots \end{aligned} \tag{28}$$

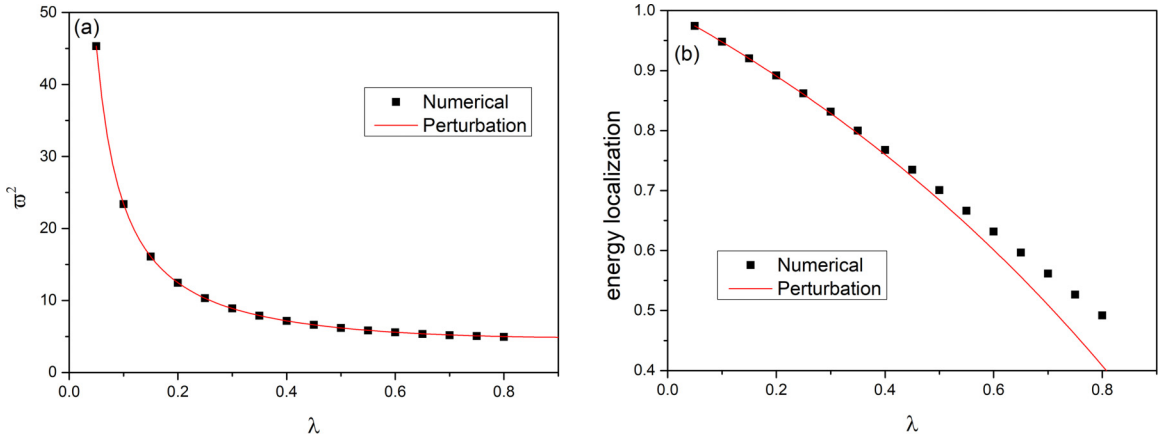

FIG. 2. Numerical solutions (points) and perturbation solutions (lines) for (a) ϖ^2 and (b) E_i/E_t at $f = 0.1$.

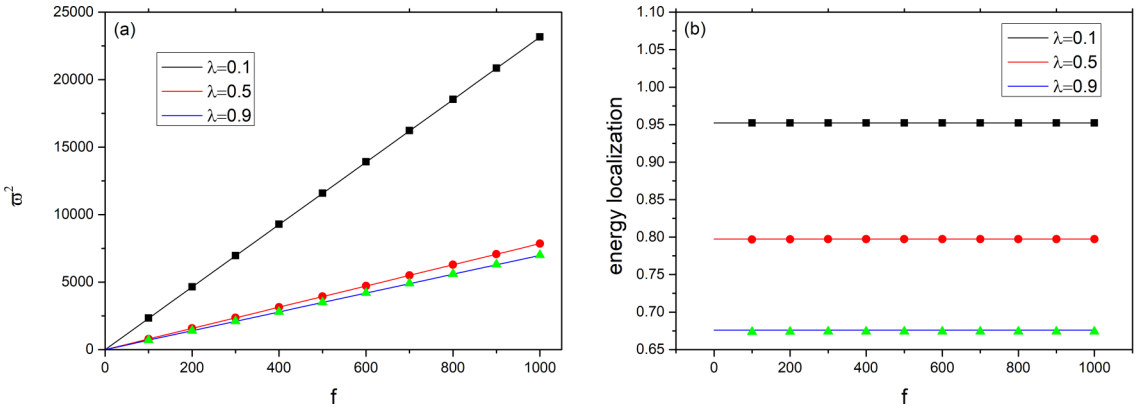

FIG. 3. Numerical solutions (points) and asymptotic solutions (lines) for (a) ϖ^2, and (b) E_i/E_t at $\lambda = 0.1, 0.5$, and 0.9.

We then have for $n = 1$,

$$v_1 = v_1(\lambda), \tag{29}$$

and $n > 1$,

$$v_n \cong \frac{\lambda}{2}\left(\frac{\lambda/2}{v_1}\right)^{\frac{3^{n-1}-3}{2}}\left(\frac{v_1}{1+v_1}\right)^{\frac{3^n-3}{2}}. \tag{30}$$

Therefore $v_1 \gg v_n$, and E_i/E_t is then approximately expressed as

$$\frac{E_i}{E_t} = \frac{v_0^2 m_0}{\sum_n v_n^2 m_n} \cong \frac{\lambda}{2v_1(\lambda)^2 + \lambda}. \tag{31}$$

In the light-mass impurity approach, where $\lambda \ll 1$, we have

$$v_1(\lambda) \cong \frac{\lambda}{2}, \tag{32}$$

$$\frac{\varpi^2}{f} \cong \frac{(1+\lambda/2)^3}{\lambda/2}, \tag{33}$$

$$v_n \cong \frac{\lambda}{2}\left(\frac{\lambda}{2+\lambda}\right)^{\frac{3^n-3}{2}}, \tag{34}$$

$$\frac{E_i}{E_t} \cong \frac{1}{1+\lambda/2}. \tag{35}$$

Equation (35) gives the energy localization limit for the anharmonic impurity modes. The pattern and the energy localization are both independent of f. Because v_n is much smaller than v_1, we hence get the approximate displacement pattern (. . . 0,-λ/2,1,-λ/2,0, . . .), which was exactly the result observed by Kivshar [14].

These asymptotic solutions are then compared with the numerical results as well, as depicted in Figs. 3 and 4. The proportional relation agrees well with the asymptotic solution, as shown in Fig. 3. Figure 4 shows that the asymptotic solutions are consistent with the numerical results for all allowed impurity masses, while the light-mass limit solution of E_i/E_t is also fitted well in the region where $\lambda < 0.4$.

Substituting Eqs. (33) and (34) into Eq. (22), the total energy takes on the following form:

$$\begin{aligned} E_t &\cong \left(1+\frac{\lambda}{2}\right)^3 \sum_n m_n \left(\frac{\lambda}{2+\lambda}\right)^{\frac{3^n-3}{2}} \times \frac{2k_2}{3k_4} \times f^2 \\ &= \left(1+\frac{\lambda}{2}\right)^3 \sum_n m_n \left(\frac{\lambda}{2+\lambda}\right)^{\frac{3^n-3}{2}} \times \frac{3k_4}{8k_2} \times {\varphi_0}^4, \end{aligned} \tag{36}$$

which shows that E_t is proportional to k_4 and ${\varphi_0}^4$. Therefore we conclude that the energy will increase dramatically with increasing vibrational amplitude.

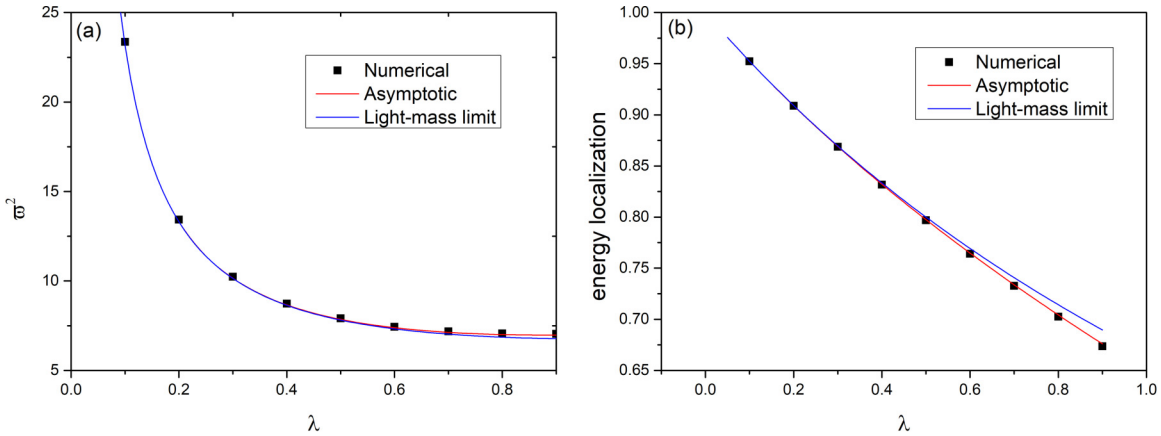

FIG. 4. Numerical solutions (points) and asymptotic solutions (lines) for (a) ϖ^2, and (b) E_i/E_t at $f = 100$. The red curves are the asymptotic solutions, and the blue curves are the light-mass limit solutions.

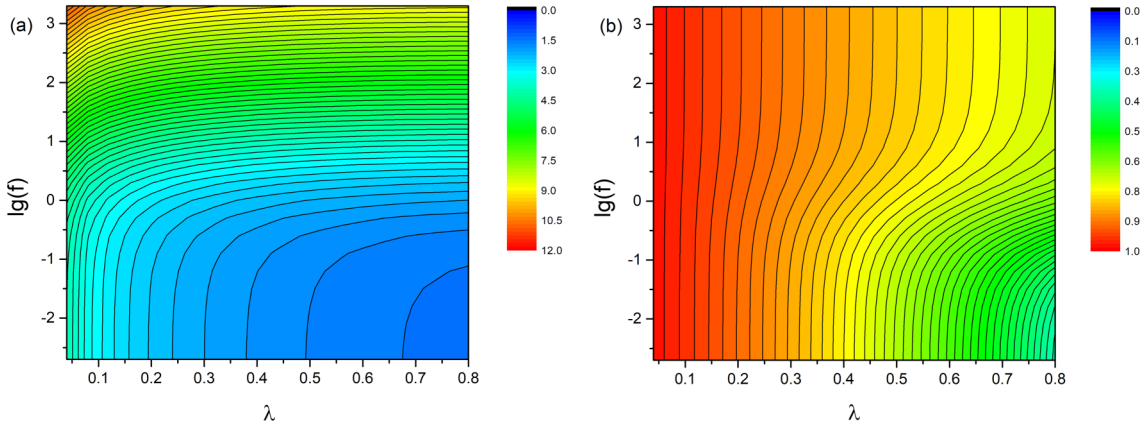

FIG. 5. (a) Logarithm of the square of the frequency, $\lg(\varpi^2)$, and (b) E_i/E_t vs λ and $\lg(f)$.

As for the more general case of f, the relationships of E_i/E_t and ϖ^2 with these parameters (i.e., λ and f) for all range of anharmonicity are shown as contour plots in Fig. 5. It reveals that both E_i/E_t and ϖ^2 increase monotonically with decreasing λ or increasing f. The contour lines show that E_i/E_t and ϖ^2 are almost independent of f in the weak-anharmonicity limit, but that they both decrease monotonically with increasing λ. By contrast, for strong anharmonicity, E_i/E_t behaves in the same manner as in the weak-anharmonicity limit case, while ϖ^2 becomes monotonically related to f. The asymptotic approach mentioned above was used to explain these phenomena.

C. Stability of the anharmonic impurity modes

In order to demonstrate the stability of the anharmonic impurity mode in the simplest way, we follow Ref. [9] to use a bifurcation diagram to draw conclusions about the mode stability by comparing the mode energies. The authors [9] used the strong-anharmonicity limit to assume that the mode is localized to only three particles. We will now improve on this result to discuss the case of 101 particles. All possible symmetric and asymmetric impurity modes [5,9] are searched by scanning f, for a fixed frequency. A bifurcation diagram of λ is obtained by scanning f in Fig. 6(a), rather than that of displacements [9]. Figure 6(a) shows that there is a critical value λ_{cr}. When $\lambda < \lambda_{cr}$ (green curve), there is only the symmetric mode, in which v_{-1} and v_1 are equal to each other. When $\lambda > \lambda_{cr}$, the symmetric mode (magenta curve) and the asymmetric mode (black curve) both exist. The asymmetric mode bifurcates at $\lambda = \lambda_{cr}$. The set of displacements of the chain is also obtained by scanning f. The total energy given by Eq. (22) is simplified by setting the unit to $\frac{2}{3}\frac{k_2^2}{k_4}\varpi^4$ and then becomes

$$E_t = \frac{f}{\varpi^2}\sum_n v_n^2 m_n. \tag{37}$$

The bifurcation curves in Fig. 6(a) are then projected to Fig. 6(b), where the black branch represents the asymmetric mode, while the blue and red branches represent the symmetric modes. It is clear that the asymmetric mode is more stable than the symmetric mode when $\lambda > \lambda_{cr}$, because the total energy of the asymmetric mode is lower for the same value of λ. At $\lambda = 1$, it reveals that the Page mode is more stable than the ST mode, which agrees well with the previous works [9,16]. It is found that λ_{cr} is a function of ϖ. We therefore plot the

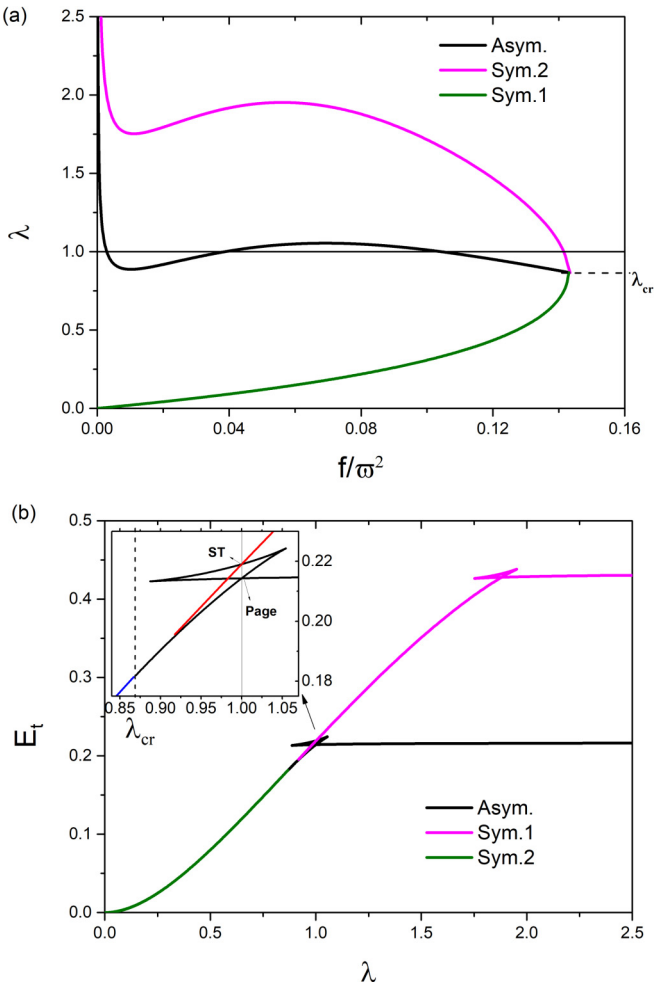

FIG. 6. (a) Bifurcation diagram for $\varpi = 100$. The green and magenta branches show the λ characteristics of the symmetric modes (denoted by Sym. 1 and 2), and the black branch shows λ for the asymmetric mode (denoted by Asym.). (b) Total energies of both the symmetric and asymmetric modes for $\varpi = 100$. The black branch is the asymmetric mode, and the red and blue branches are symmetric modes.

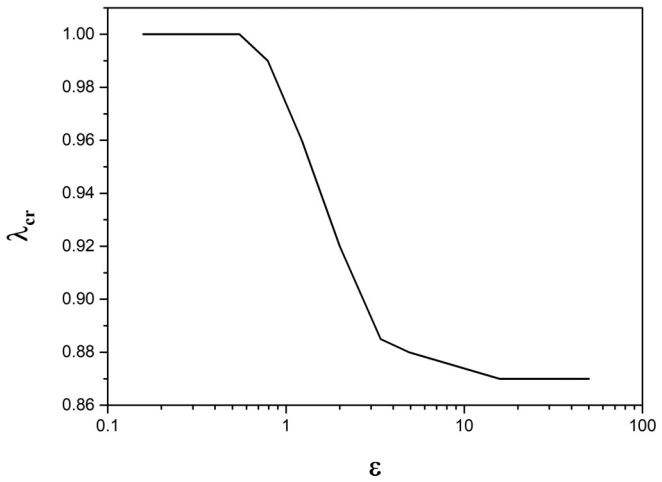

FIG. 7. Critical value λ_{cr} vs frequency variable ε.

relationship between them as shown in Fig. 7 by introducing another variable ε for describing the relationship between ϖ and ϖ_m [5],

$$\varepsilon = \sqrt{\frac{\varpi^2}{\varpi_m^2}} - 1. \tag{38}$$

Figure 7 shows that λ_{cr} decreases with increasing ε and eventually reaches 0.87 at the high-frequency limit. Kovalev reported that $\lambda_{cr} = 0.91$ at the high-frequency limit, which shows good agreement with our results [5,9]. The relationship between λ_{cr} and ε has not been reported in these previous works because only three or four neighboring particles were taken into account [5,9].

The stability of the anharmonic impurity modes must be also affected by the environmental fluctuations, e.g., decay processes or energy exchanges with the substrate [17]. However, in our model, the rotating-wave approximation is used, in which only one frequency is taken into account, so there are no decay processes. Meanwhile, the isolated chain is used in our model, so these energy exchanges are all beyond its scope.

IV. CONCLUSIONS

In summary, we have presented numerical and asymptotic solutions for the symmetric anharmonic impurity mode of a 1D chain. In the weak-anharmonicity limit, the energy localization varies linearly with respect to f. In the strong-anharmonicity limit, the asymptotic solutions show that the energy localization reduces to a function only related to λ. The total energy of the localized mode is proportional to k_4 and ${\varphi_0}^4$. The numerical results for the whole range of anharmonicity reveal that the rate of energy localization increases monotonically with decreasing λ or increasing f.

The stability of both symmetric and asymmetric modes was studied using a bifurcation diagram. It is found that only the symmetric mode is allowed when $\lambda < \lambda_{cr}$. When $\lambda > \lambda_{cr}$, both modes exist, but the asymmetric mode is the more stable one. It shows that λ_{cr} is then found to be a function of frequency, with a value of 1 at low frequency, and a limit value of 0.87 at high frequency.

ACKNOWLEDGMENTS

We thank A. J. Sievers, J. N. Teixeira Rabelo, and Xing-Bin Huang for numerous discussions and for their helpful advice. We thank Professor Lars Q English for the help of improving the English of this paper. This work was supported by the National Natural Science Foundation of China (Grants No. 21673211 and No. 11372053) and the Science Challenge Project, No. TZ2016001.

X.-L.C. and G.-B.Z. contributed equally to this work.

[1] I. P. Maradudin, A. A. Montroll, E. W. Weiss, and G. S. Ipatova, *Theory of Lattice Dynamics in the Harmonic Approximation* (Academic Press, New York, 1971).
[2] A. M. Kosevich and A. S. Kovalev, Sov. Phys. JETP **40**, 891 (1974).
[3] A. J. Sievers and S. Takeno, Phys. Rev. Lett. **61**, 970 (1988).
[4] J. B. Page, Phys. Rev. B **41**, 7835 (1990).
[5] Y. S. Kivshar, F. Zhang, and A. S. Kovalev, Phys. Rev. B **55**, 14265 (1997).
[6] J. Cuevas, F. Palmero, J. F. R. Archilla, and F. R. Romero, J. Phys. A **35**, 10519 (2002).
[7] G. P. Tsironis and S. Aubry, Phys. Rev. Lett. **77**, 5225 (1996).
[8] K. Ø. Rasmussen, S. Aubry, A. R. Bishop, and G. P. Tsironis, Eur. Phys. J. B **15**, 169 (2000).
[9] A. S. Kovalev, F. Zhang, and Y. S. Kivshar, Phys. Rev. B **51**, 3218 (1995).
[10] R. Sarkar, Commun. Nonlinear Sci. Numer. Simul. **15**, 3248 (2010).
[11] R. Sarkar and B. Dey, Pramana - J. Phys. **70**, 1023 (2008).
[12] A. J. Sievers, S. A. Kiselev, and S. R. Bickham, J. Lumin. **58**, 37 (1994).
[13] Y. S. Kivshar, Phys. Lett. A **173**, 172 (1993).
[14] Y. S. Kivshar, Phys. Lett. A **161**, 80 (1991).
[15] M. Hornquist and R. Riklund, Phys. Rev. B **55**, 875 (1997).
[16] O. A. Chubykalo, A. S. Kovalev, and O. V. Usatenko, Phys. Lett. A **178**, 129 (1993).
[17] O. M. Braun and Y. S. Kivshar, Phys. Rev. B **43**, 1060 (1991).